

On the nature of the mass-gap object in the GW190814 event

Luiz L. Lopes^{1,*} and Debora P. Menezes²

¹*Centro Federal de Educação Tecnológica de Minas Gerais Campus VIII; CEP 37.022-560, Varginha - MG - Brasil*

²*Departamento de Física, CFM - Universidade Federal de Santa Catarina; C.P. 476, CEP 88.040-900, Florianópolis, SC, Brasil*
(Dated: May 18, 2022)

In this work, we make a very extensive study on the conditions that allow the mass-gap object in the GW190814 event to be faced as a degenerate star instead of a black hole. We begin revisiting some parametrizations of the Quantum Hadrodynamics (QHD) and then study under which conditions the hyperons are present in such a massive star. Afterwards, using a vector MIT based model, we study if self-bound quark stars, satisfying the Bodmer-Witten conjecture fulfills all the observational constraints. Finally, we study hybrid stars within a Maxwell construction and check for what values of the bag, as well as the vector interaction, a quark core star with only nucleons, and with nucleons admixed with hyperons can reach at least $2.50 M_{\odot}$. We conclude that, depending on the choice of parameters, none of the possibilities can be completely ruled out, i.e., the mass-gap object can be a hadronic (either nucleonic or hyperonic), a quark or a hybrid star, although some cases are more probable than others.

I. INTRODUCTION

In 2019, the GW190814 [1] was detected as the result of a coalescence of a $25.6 M_{\odot}$ black-hole and a compact object of mass $2.5\text{--}2.67 M_{\odot}$, which can be either the most massive neutron star or the least massive black hole ever seen, once it lies in the region known as mass-gap, in between 2.5 and $5 M_{\odot}$.

The possibility of the mass-gap object being a neutron star has already been studied in previous works. For instance, in ref. [2] the influence of the symmetry energy was studied, and a pure nucleonic neutron star with mass around $2.75 M_{\odot}$ was obtained. The possibility of dark matter admixed in pure nucleonic neutron star was studied in ref. [3], and a maximum mass of $2.50 M_{\odot}$ was shown to be possible. In refs. [4, 5] the authors discussed the possibility of hybrid stars and hadronic neutron stars with hyperons. They have concluded that the mass-gap object can be a hybrid star only if the star is fast rotating [4]. Nevertheless, the presence of hyperons seems to be unlikely even in the Kepler frequency limit [4, 5]. Using the generic constant-sound-speed (CSS) parametrization, ref. [6] shows that a hybrid star with maximum mass above $2.50 M_{\odot}$ is possible, even in the static case.

On the other hand, ref. [7] rules out the possibility of quark-hadron phase transition, at least in the non-rotating case. But, according to a model-independent analysis based on the sound velocity, quark-cores are indeed expected inside massive stars [8]. Δ -admixed neutron stars were studied in ref. [9] and can account for the mass-gap object only in the Keplerian limit, ruling out static stars with Δ resonances. In these studies, no static neutron star with exotic matter fulfills the mass-gap object constraint.

Another possibility is the mass-gap object being a self-bound strange star satisfying the Bodmer-Witten

conjecture [10, 11]. This possibility was studied in refs. [12, 13], where the authors consider a color superconducting quark matter, and also in ref. [14], where the authors consider a repulsive bag model with dynamically generated gluon mass. Moreover, using CFL NJL model, ref. [15] also produces quark stars with masses above $2.50 M_{\odot}$.

In this work, we study if the mass gap object in the GW190814 event can be a purely nucleonic neutron star, a nucleonic admixed hyperon neutron star, a self-bound quark star satisfying the Bodmer-Witten conjecture [10, 11], a hybrid star with nucleons and a quark core or a hybrid star with nucleons, hyperons and a quark core. The paper is organized as follows:

In sec. II, we present the Quantum Hadrodynamics (QHD) model that simulates the interaction between nucleons as well hyperons. We show how to construct the equation of state (EoS) and discuss some parametrizations in the light of both, the GW190814 event, as well as the necessary constraints that satisfy symmetric nuclear matter properties. We then discuss how hyperons affect the EoS and in what conditions hyperonic neutron stars can still reach at least $2.50 M_{\odot}$. Constraints related to the radius and tidal deformability of the canonical $1.4 M_{\odot}$ neutron stars are also discussed.

In sec. III, the vector MIT bag model is presented and we discuss the possibility of very massive self-bound quark stars. Two parametrizations for the quark-quark interaction are discussed: an universal coupling, where the vector field of all the quarks has the same strength, and a coupling deduced from symmetry group arguments. The results are again compared with the constraints imposed by the radius and the tidal deformability of the canonical star.

In sec. IV we construct a hybrid branch stability window; i.e, we obtain values for the bag and for the vector field, where a stable hybrid star with a mass above $2.50 M_{\odot}$ is possible. We also calculate the size and the mass of the quark core of these hybrid stars. At the end, the conclusions are drawn.

* llopes@cefetmg.br

II. THE QHD MODEL

To simulated the interaction between baryons in dense cold matter, we use an extended version of the QHD model, whose Lagrangian density reads [16, 17]:

$$\begin{aligned}\mathcal{L}_{QHD} = & \bar{\psi}_B[\gamma^\mu(i\partial_\mu - g_{B\omega}\omega_\mu - g_{B\rho}\frac{1}{2}\vec{\tau} \cdot \vec{\rho}_\mu) + \\ & -(M_B - g_{B\sigma}\sigma)]\psi_B - U(\sigma) + \\ & + \frac{1}{2}(\partial_\mu\sigma\partial^\mu\sigma - m_s^2\sigma^2) - \frac{1}{4}\Omega^{\mu\nu}\Omega_{\mu\nu} + \frac{1}{2}m_v^2\omega_\mu\omega^\mu + \\ & + \frac{1}{2}m_\rho^2\vec{\rho}_\mu \cdot \vec{\rho}^\mu - \frac{1}{4}P^{\mu\nu} \cdot P_{\mu\nu} + \mathcal{L}_{\omega\rho} + \mathcal{L}_\phi, \quad (1)\end{aligned}$$

in natural units. ψ_B is the baryonic Dirac field, where B can stand either for nucleons only (N) or can run over nucleons (N) and hyperons (H). The σ , ω_μ and $\vec{\rho}_\mu$ are the mesonic fields, while $\vec{\tau}$ are the Pauli matrices. The g 's are the Yukawa coupling constants that simulate the strong interaction, M_B is the baryon mass, m_s , m_v and m_ρ are the masses of the σ , ω and ρ mesons respectively. The $U(\sigma)$ is the self-interaction term introduced in ref. [18]:

$$U(\sigma) = \frac{1}{3}\lambda\sigma^3 + \frac{1}{4}\kappa\sigma^4,$$

and $\mathcal{L}_{\omega\rho}$ is a non-linear ω - ρ coupling interaction as in ref. [17]:

$$\mathcal{L}_{\omega\rho} = \Lambda_{\omega\rho}(g_{N\rho}^2\vec{\rho}^\mu \cdot \vec{\rho}_\mu)(g_{N\omega}^2\omega^\mu\omega_\mu), \quad (2)$$

which is necessary to correct the slope of the symmetry energy (L) and has a strong influence on the radii and tidal deformation of the neutron stars [19, 20]; \mathcal{L}_ϕ is related the strangeness hidden ϕ vector meson, which couples only with the hyperons (H), not affecting the properties of symmetric nuclear matter:

$$\mathcal{L}_\phi = g_{H\phi}\bar{\psi}_H(\gamma^\mu\phi_\mu)\psi_H + \frac{1}{2}m_\phi^2\phi_\mu\phi^\mu - \frac{1}{4}\Phi^{\mu\nu}\Phi_{\mu\nu}, \quad (3)$$

as pointed in ref. [21, 22], this vector channel is crucial to obtain massive hyperonic neutron stars.

As neutron stars are stable macroscopic objects, we need to describe a neutral, chemically stable matter and hence, leptons are added as free Fermi gases, whose Lagrangian density is the usual one.

$$\mathcal{L}_l = \bar{\psi}_l[\gamma^\mu(i\partial_\mu - m_l)]\psi_l.$$

To solve the equations of motion, we use the mean field approximation (MFA), where the meson fields are replaced by their expectation values. Applying the Euler-Lagrange formalism, and using the quantization rules ($E = \partial^0$, $k = i\partial^j$) we easily obtain the eigenvalue for the energy:

$$E_B = \sqrt{k^2 + M_B^{*2}} + g_{B\omega}\omega_0 + g_{B\phi}\phi_0 + \frac{\tau_{3B}}{2}g_{B\rho}\rho_0, \quad (4)$$

where $M_B^* \equiv M_B - g_{B\sigma}\sigma_0$ is the effective baryon mass and τ_{3B} assumes the value of +1 for p, Σ^+ , and Ξ^0 ; zero for Λ^0 and Σ^0 ; and -1 for n, Σ^- and Ξ^- . For the leptons, we have:

$$E_l = \sqrt{k^2 + m_l^2}, \quad (5)$$

and the mesonic fields in MFA are given by:

$$\begin{aligned}m_\sigma^2\sigma_0 + \lambda\sigma_0^2 + \kappa\sigma_0^3 &= \sum_B g_{B\sigma}n_B^s, \\ (m_\omega^2 + 2\Lambda_v\rho_0^2)\omega &= \sum_B g_{B\omega}n_B, \\ m_\phi^2\phi_0 &= \sum_B g_{B\phi}n_B, \\ (m_\rho^2 + 2\Lambda_v\omega_0^2)\rho_0 &= \sum_B g_{B\rho}\frac{\tau_{3B}}{2}n_B,\end{aligned} \quad (6)$$

where $\Lambda_v \equiv \Lambda_{\omega\rho}g_{N\omega}^2g_{N\rho}^2$, and n_B^s and n_B are, respectively, the scalar density and the number density of the baryon B . Finally, applying Fermi-Dirac statistics to baryons and leptons and with the help of Eq. (6), we can write the total energy density as [23]:

$$\begin{aligned}\epsilon = & \sum_B \frac{1}{\pi^2} \int_0^{k_{Bf}} dk k^2 \sqrt{k^2 + M_B^{*2}} + \\ & + \frac{1}{2}m_\sigma^2\sigma_0^2 + \frac{1}{2}m_\omega^2\omega_0^2 + \frac{1}{2}m_\phi^2\phi_0^2 + \frac{1}{2}m_\rho^2\rho_0^2 + \\ & + U(\sigma_0) + 3\Lambda_v\omega_0^2\rho_0^2 + \\ & + \sum_l \frac{1}{\pi^2} \int_0^{k_{lf}} dk k^2 \sqrt{k^2 + m_l^2},\end{aligned} \quad (7)$$

and the pressure is easily obtained by thermodynamic relations: $p = \sum_f \mu_f n_f - \epsilon$, where the sum runs over all the fermions and μ_f is the corresponding chemical potential. Now, to determine each particle population, we impose that the matter is β stable and has total electric net charge equals to zero.

A. Parametrization

Our knowledge of nuclear physics took a great leap in the last decade. From nuclear masses analysis [24], passing through nuclear resonances [25, 26], and heavy ion collisions (HIC) [27]; we are able to constraint five parameters of the symmetric nuclear matter at the saturation point: the saturation density itself (n_0), the effective nucleon mass (M_N^*/M_N), the incompressibility (K), the

binding energy per baryon (B/A) [28] and the symmetry energy (S_0). The experimental values of these five parameters are taken from two extensive review articles, ref. [29, 30] and are presented in Tab. I. Besides these five parameters, a sixth one is nowadays a matter of open discussion: the symmetry energy slope, L . For instance, an upper limit for L of 54.6 MeV, 61.9 MeV and 66 MeV was presented in ref. [31–33] respectively. These values are in strong contrast with recent measurements. For instance,

an upper limit of 117.5 MeV was found in ref. [34], in a study about the spectra of pions in intermediate energy collisions, while PREX2 results not only presented an upper limit as high as 143 MeV, but also an inferior limit of only 69 MeV [35]. Such high inferior limit makes PREX2 constraint difficult to reconcile with the results obtained in ref. [31–33]. In order to maintain consistency with the other constraints, we have opted to use here $36 \text{ MeV} < L < 86.8 \text{ MeV}$ as a constraint, once it was pointed out in ref. [30].

	Parameters		Constraints	This model
$g_{N\sigma}$	10.0944	$n_0 \text{ (fm}^{-3}\text{)}$	0.148 - 0.170	0.150
$g_{N\omega}$	12.8065	M^*/M	0.56 - 0.75	0.594
$g_{N\rho}$	14.441	$K \text{ (MeV)}$	220 - 260	258
κ	-10.8093 (fm $^{-1}$)	$S_0 \text{ (MeV)}$	30.0 - 35.0	30.7
λ	-30.1486	$L \text{ (MeV)}$	36 - 86.8	42
$\Lambda_{\omega\rho}$	0.045	$B/A \text{ (MeV)}$	15.8 - 16.5	16.31

TABLE I. Parameters of the modified NL3* model [38], utilized in this work and their prediction for the symmetric nuclear matter at the saturation density; the phenomenological constraints are taken from ref. [29, 30],

It is crystal clear that we need a very stiff equation of state (EoS) in order to obtain at least a $2.50 M_\odot$ star. There are few QHD models that are able to produce such massive neutron star and still be in agreement with the constraints presented in Tab. I. We can highlight the NL3 [36], which although a little outdated, is still used in very recent studies [2, 3, 37]; its updated version, the so-called NL3* [38]; the NL-RA1 [39]; and the recent BigApple parametrization [40]. But, of all of these parametrizations, only the BigApple has a symmetry energy slope consistent with the constraint presented in ref. [30], $36 \text{ MeV} < L < 86.8 \text{ MeV}$. Nevertheless, with the help of the non-linear $\omega - \rho$ coupling given in Eq. (2), we can redefine the symmetry energy slope without affecting any of the others properties of the symmetric nuclear matter. A more serious issue is the incompressibility (K). Assuming that K lies between 240 ± 20 , as pointed out in ref. [30], only the NL3* and the BigApple fulfill this constraint. As the BigApple produces a maximum star mass of $2.60 M_\odot$ and the NL3* has a maximum mass of $2.75 M_\odot$, we use in this work a modified version of the NL3*, which includes the $\omega - \rho$ coupling. All the parameters are displayed in Tab I.

Once the parametrization of the nuclear matter is settled, we need to focus on the parametrization of the hyperon-meson coupling constants. There is little information about the hyperon interaction. One of the few well known quantity is the Λ^0 potential depth, $U_\Lambda = -28 \text{ MeV}$. The hyperon potential depth is defined as [28]:

$$U_Y = g_{Y\omega}\omega_0 - g_{Y\sigma}\sigma_0. \quad (8)$$

The potential depth for the Σ and the Ξ are known with less precision. In this work we use the standard value $U_\Sigma = +30 \text{ MeV}$ and $U_\Xi = -4 \text{ MeV}$, which was recently favored by lattice QCD calculations [41]. Nevertheless, the knowledge of the hyperon potential depth only solves partially the problem once from Eq. (8), different combinations of $g_{Y\omega}$ and $g_{Y\sigma}$ can produce the same value for the potential depth. And, as pointed in ref. [28], different values of the hyperon-meson coupling constants can lead to a maximum mass difference up to 100%. The situation becomes even worse, as the potential depth give us no information about the hyperon-meson coupling constants with the ρ and the ϕ mesons.

An alternative is the use of symmetry group arguments. For instance, all coupling constants for the vector mesons can be fixed simultaneously by applying SU(6) symmetry group [21, 22]. However, in general, SU(6) symmetry group produces neutron stars not as massive as desired in the present investigation. We can solve this problem by breaking the SU(6) symmetry group into a more general SU(3) flavor symmetry group. In this case, the coupling constant for the vector meson depends of a single parameter, α . Therefore we have for the ω meson [23, 42, 43]:

$$\frac{g_{\Lambda\omega}}{g_{N\omega}} = \frac{4 + 2\alpha}{5 + 4\alpha}, \quad \frac{g_{\Sigma\omega}}{g_{N\omega}} = \frac{8 - 2\alpha}{5 + 4\alpha}, \quad \frac{g_{\Xi\omega}}{g_{N\omega}} = \frac{5 - 2\alpha}{5 + 4\alpha},$$

for the ϕ meson:

$$\begin{aligned} \frac{g_{\Lambda\phi}}{g_{N\omega}} &= \sqrt{2} \left(\frac{2\alpha - 5}{5 + 4\alpha} \right), & \frac{g_{\Sigma\phi}}{g_{N\omega}} &= -\sqrt{2} \left(\frac{2\alpha_v + 1}{5 + 4\alpha} \right), \\ \frac{g_{\Xi\phi}}{g_{N\omega}} &= -\sqrt{2} \left(\frac{2\alpha + 4}{5 + 4\alpha} \right), & \frac{g_{N\phi}}{g_{N\omega}} &= 0, \end{aligned}$$

and finally for the ρ meson:

$$\frac{g_{\Sigma\rho}}{g_{N\rho}} = 2\alpha, \quad \frac{g_{\Xi\rho}}{g_{N\rho}} = 2\alpha_v - 1, \quad \frac{g_{\Lambda\rho}}{g_{N\rho}} = 0. \quad (9)$$

We next choose some arbitrary values for α and calculate the vector meson coupling constants, while the scalar meson coupling constants are fixed in order to reproduce realistic values of the potential depth, as mentioned above: $U_\Lambda = -28$ MeV, $U_\Sigma = +30$ MeV and $U_\Xi = -4$ MeV. The calculated coupling constants are displayed in Tab. II, while we plot in Fig. 1 the particle population for these values of α . Notice that for $\alpha = 1$ the group SU(6) is recovered.

-	$\alpha = 1.00$	$\alpha = 0.75$	$\alpha = 0.50$	$\alpha = 0.25$
$g_{\Lambda\omega}/g_{N\omega}$	0.667	0.687	0.714	0.75
$g_{\Sigma\omega}/g_{N\omega}$	0.667	0.812	1.00	1.25
$g_{\Xi\omega}/g_{N\omega}$	0.333	0.437	0.571	0.75
$g_{\Lambda\phi}/g_{N\omega}$	-0.471	-0.619	-0.808	-1.06
$g_{\Sigma\phi}/g_{N\omega}$	-0.471	-0.441	-0.404	-0.354
$g_{\Xi\phi}/g_{N\omega}$	-0.943	-0.972	-1.01	-1.06
$g_{\Sigma\rho}/g_{N\rho}$	2.0	1.5	1.0	0.5
$g_{\Xi\rho}/g_{N\rho}$	1.0	0.5	0.0	-0.5
$g_{\Lambda\sigma}/g_{N\sigma}$	0.613	0.629	0.651	0.679
$g_{\Sigma\sigma}/g_{N\sigma}$	0.461	0.578	0.730	0.930
$g_{\Xi\sigma}/g_{N\sigma}$	0.279	0.374	0.428	0.616

TABLE II. Hyperon-meson coupling constants for different values of α . When we impose $\alpha = 1$ we recover the group SU(6).

We can see that for all values of α , the only hyperons present are the Λ^0 and the Ξ^- . Also, for all values of α , the Λ^0 is the first hyperon to appear, at densities around 0.33 fm^{-3} . For the SU(6) parametrization, the potentials depth are less repulsive at high density. Due to this fact, the hyperons are favored, resulting in two interesting features: the Λ^0 becomes the most populous particle at densities around 0.73 fm^{-3} , matter is practically deleptonized, and the electric charge neutrality is reached with equal proportions of protons and Ξ^- hyperons. For $\alpha = 0.75$, the matter is also deleptonized, but at higher densities. For lower values, the potentials depth are already too repulsive, and electrons and muons are always present.

A more clever way to understand the variation of strangeness content particle is, instead of looking at the individual hyperon population, looking at the strangeness fraction, f_s , defined as:

$$f_s = \frac{1}{3} \frac{\sum n_i |s_i|}{n}, \quad (10)$$

where s_i is the strangeness of the i -th baryon. The results are plotted in Fig. 2. As we can see, there is a direct relation between α and the strangeness fraction, as also pointed out in ref. [43]. When we move away from SU(6) we increase the repulsion of the hyperons, by increasing the $Y - \omega$ and the $Y - \phi$ coupling constants as shown in Tab. II. This reduces the hyperon population at high densities, reducing the strangeness fraction.

Now we use the EoS for different values of α as input to solve the TOV equations [44]:

$$\begin{aligned} \frac{dp}{dr} &= \frac{-GM(r)\epsilon(r)}{r^2} \left[1 + \frac{p(r)}{\epsilon(r)} \right] \\ &\times \left[1 + \frac{4\pi p(r)r^3}{M(r)} \right] \left[1 - \frac{2GM(r)}{r} \right]^{-1}, \\ \frac{dM}{dr} &= 4\pi r^2 \epsilon(r). \end{aligned} \quad (11)$$

The EoS as well the mass-radius relation of the TOV solution are displayed in Fig. 3, where we use the BPS EoS to simulate the neutron star crust [45]. As can be seen, there is a clear relation between the value of α , the strangeness fraction, f_s , the EoS and the maximum mass. The lower the value of the α , the lower the value of f_s , which produces stiffer EoS, as well as more massive stars. In the light of the GW190814 event, we can see that this mass-gap object not only can be a pure nucleonic neutron star, but also a hyperon admixed star, if $\alpha < 0.75$. For $\alpha \geq 0.75$, the maximum mass lies below $2.50 M_\odot$. Also, as the Λ^0 onset happens around 0.33 fm^{-3} for all values of α , no hyperonic neutron stars with mass below $1.66 M_\odot$ is possible.

We can also discuss our results in the light of some observational astronomical constraints. One of the hot topics in modern days is the radius of the canonical star, $M = 1.40 M_\odot$. However, as pointed in ref. [19], the radius of the canonical star strongly depends of the symmetry energy slope, L . And, as discussed earlier, the high uncertainty about its value will obviously affect the uncertainty of the radius. For instance, in ref. [46], a very small upper limit, of only 11.1 km was presented. Another small value of 11.9 km was also pointed in ref. [47], while in ref. [48] an upper limit of 12.45 km was deduced. More recently, results obtained from Bayesian analysis indicate that the radius of the canonical star lies between 10.8 km and 13.2 km in ref. [49]; and 11.3 km to 13.5 km in ref. [50]; whilst results coming from the NICER x-ray telescope points out that $R_{1.4}$ lies between 11.52 km and 13.85 km from ref. [51] and between 11.96 km and 14.26 km from ref. [52]. State-of-the-art theoretical results at low and high baryon density point to an upper limit of $R_{1.4} < 13.6 \text{ km}$ [53]. Finally, PREX2 results [35] indicate that the radius of the canonical star lies between 13.25

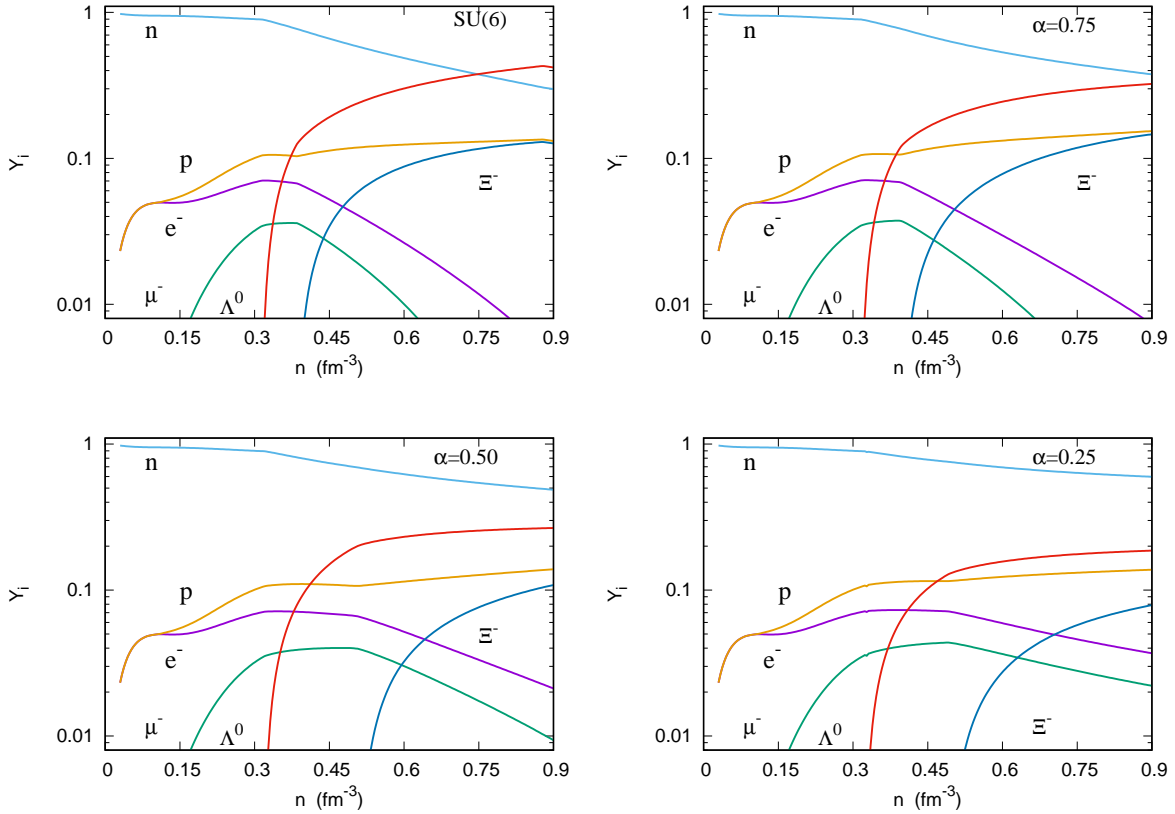


FIG. 1. (Color online) Particle population for the SU(6) group and different values of α .

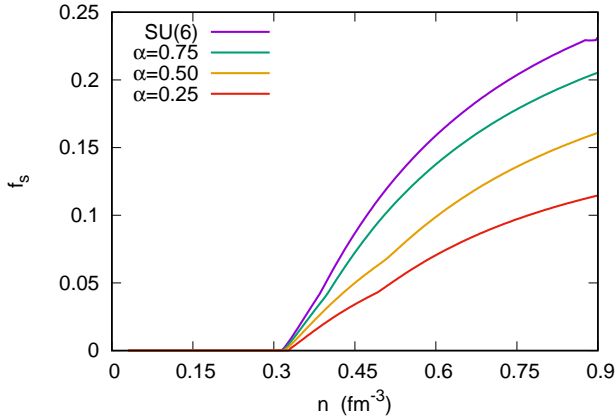


FIG. 2. (Color online) Strangeness fraction as a function of α .

$\text{km} < R_{1.4} < 14.26 \text{ km}$. This constraint is mutually exclusive with the result presented in refs. [46–49].

Notwithstanding, in this work we use as a constraint the radius of the canonical star between $12.2 \text{ km} < R_{1.4} < 13.7 \text{ km}$, as presented in ref. [1]. The reason why we choose this value over all the others discussed above is because it is derived from the GW190814 event

itself, the subject of the present work. As, in our study no hyperon is present in a $1.4 M_{\odot}$ star, its radius for all values of α is 13.38 km . Such value is in agreement with our main constraint from ref. [1], as well as it is in agreement with NICER results [51, 52], Bayesian analysis [50], PREX2 [35], and state-of-the-art theoretical results [53]. However, it is in disagreement with the results presented in ref. [46–49].

Another important quantity and constraint is the so-called dimensionless tidal deformability parameter Λ . If we put an extended body in an inhomogeneous external field it will experience different forces throughout its extent. The result is a tidal interaction. The tidal deformability of a compact object is a single parameter λ that quantifies how easily the object is deformed when subjected to an external tidal field. A larger tidal deformability indicates that the object is easily deformable. On the opposite side, a compact object with a small tidal deformability parameter is more compact and more difficult to deform. The tidal deformability is defined as the ratio between the induced quadrupole Q_{ij} and the perturbing tidal field \mathcal{E}_{ij} that causes the perturbation:

$$\lambda = -\frac{Q_{ij}}{\mathcal{E}_{ij}}. \quad (12)$$

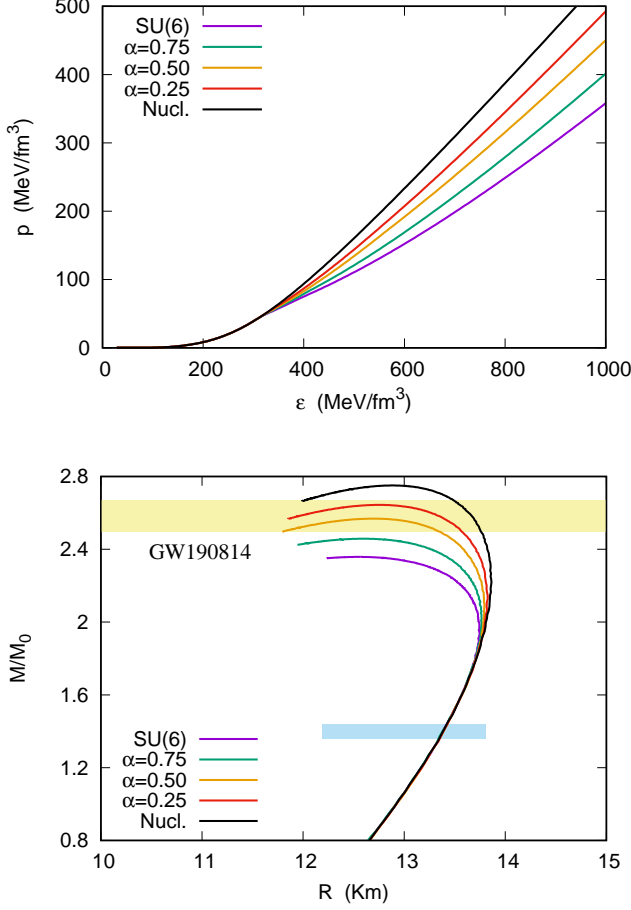


FIG. 3. (Color online) Top: EoS for the different values of the parameter α . Bottom: Mass radius relation for pure nucleonic and hyperonic stars. The yellowish hatched area refers to the uncertainty of the lower mass compact object present in the GW190814 event, while the blueish hatched area is the uncertainty about the radius of the $1.4M_{\odot}$ star. Both constraints are taken from ref. [1]. The radius of all canonical stars is 13.38 km.

However, in the literature is more commonly found the dimensionless tidal deformability parameter Λ defined as:

$$\Lambda \equiv \frac{\lambda}{M^5} \equiv \frac{2k_2}{3C^5}, \quad (13)$$

where M is the compact object mass and $C = GM/R$ is its compactness. The parameter k_2 is called the second (order) Love number:

$$k_2 = \frac{8C^5}{5} (1 - 2C)^2 [2 + 2C(y_R - 1) - y_R] \times \{2C[6 - 3y_R + 3C(5y_R - 8)] + 4C^3[13 - 11y_R + C(3y_R - 2) + 2C^2(1 + y_R)] + 3(1 - 2C)^2[2 - y_R + 2C(y_R - 1)]\} \ln(1 - 2C)^{-1}, \quad (14)$$

where $y_R = y(r = R)$ and $y(r)$ is obtained by solving:

$$y \frac{dy}{dr} + y^2 + yF(r) + r^2Q(r) = 0. \quad (15)$$

Eq. (15) must be solved coupled with the TOV equations, Eq. (11). The coefficients $F(r)$ and $Q(r)$ are given by:

$$F(r) = \frac{1 - 4\pi G r^2 [\epsilon(r) - p(r)]}{E(r)}, \quad (16)$$

$$Q(r) = \frac{4\pi G}{E(r)} \left[5\epsilon(r) + 9p(r) + \frac{\epsilon(r) + p(r)}{\partial p / \partial \epsilon} - \frac{6}{4\pi G r^2} \right] - 4 \left[\frac{G[M(r) + 4\pi r^3 p(r)]}{r^2 E(r)} \right]^2, \quad (17)$$

where $E(r) = (1 - 2GM(r)/r)$. Additional discussion about the theory of the tidal deformability, as well as the tidal Love numbers are beyond the scope of this work and can be found in ref. [15, 54–57] and references therein.

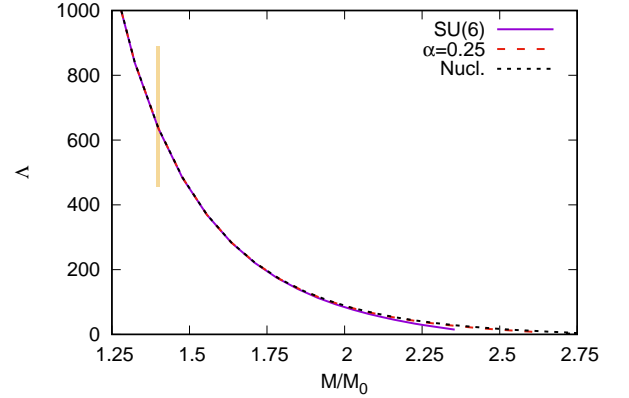


FIG. 4. (Color online) Dimensionless tidal parameter for pure nucleonic stars, as well for two values of α . The hatched area refers to the uncertainty of the tidal deformability parameter deduced from the GW190814 event [1].

We display in Fig. 4 the tidal deformability parameter Λ as a function of the star mass of pure nucleonic stars as well as for hyperonic stars with two values of α . Exactly as in the case of the radius, the dimensionless tidal parameter of the canonical star, $\Lambda_{1.4}$ can be used as a constraint. An upper limit of 860 was found in ref. [50]. A close limit, $\Lambda_{1.4} < 800$ was pointed in ref. [57]. In ref. [49], an upper limit of 686 was deduced from Bayesian analysis. On the other hand, two mutually exclusive constraints are presented in ref. [54], which proposed a limit between $70 < \Lambda_{1.4} < 580$, and the PREX2 inferred values, whose limit lies between $642 < \Lambda_{1.4} < 955$ [35]. Here, as done in the case of the radius, we use the values $458 < \Lambda_{1.4} < 889$ as a constraint, once it

was derived from the GW190814 event itself and is presented in ref. [1]. As no hyperons are present in a $1.4M_\odot$ star, with the choice of parameters used in this study, all canonical stars have the same value for the $\Lambda_{1.4} = 644$. This value is in agreement with the main constraint from ref. [1], as well as with all the others, except for the one presented in ref. [54].

Another important quantity of dense cold nuclear matter is the speed of sound, defined as:

$$v_s^2 = \frac{\partial p}{\partial \epsilon}. \quad (18)$$

The speed of sound is related to the stiffness of the EoS, and can give us important insight about the internal composition of the neutron star. In general, for a pure nucleonic neutron star, the speed of sound grows monotonically. However, the onset of new degrees of freedom can produce a non-trivial behaviour and the speed of the sound can present maxima and minima. The speed of the sound also acts as a constraint, once super-luminal values, $v_s^2 > 1$, violate Lorentz symmetry. Moreover, due to the conformal symmetry of the QCD, perturbative QCD (pQCD) predicts an upper limit $v_s^2 < 1/3$ at very high densities, $n > 40 n_0$ [59]. Such high density is far beyond those found in the neutron star interiors.

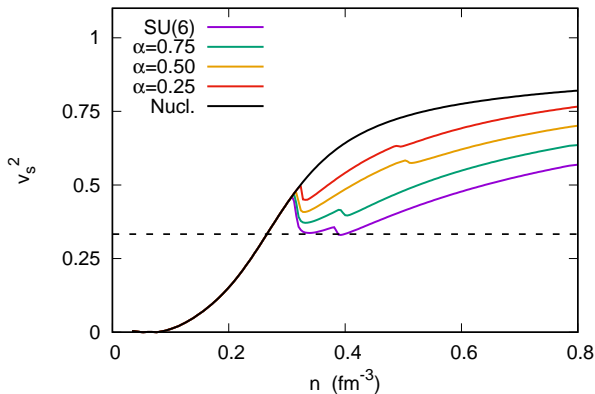


FIG. 5. (Color online) Square of the speed of sound for pure nucleonic and hyperonic matter for different values of α . The horizontal line is the conformal limit predicted by pQCD.

The speed of the sound may also be linked to the size of the quark core of a hybrid star. As recently pointed out

in ref. [8], the speed of the sound of the quark matter is closely related to the mass and radius of the quark core in hybrid stars. The authors found that if the conformal bound ($v_s^2 < 1/3$) is not strongly violated, massive neutron stars are predicted to have sizable quark-matter cores. We show in the fig. 5 the square of the speed of the sound for pure nucleonic matter, as well as for hyperonic matter for different values of α .

As can be seen, all of our models are causal, $v_s^2 < 1$. This was expected, since we are dealing with a relativistic model. The onset of hyperons breaks the monotonic behaviour and reduces the speed of the sound. The higher the value of α , the lower is the speed of the sound. Nevertheless, the conformal limit is always violated.

The last constraint for hadronic neutron stars presented in this work is the minimum mass that enables the direct Urca (DU) process. As pointed in ref. [60], any acceptable EoS shall not allow the direct Urca process to occur in neutron stars with masses below $1.5 M_\odot$. Therefore, we also use this value as constraint. The trigger to the nucleonic direct Urca channel is directly related to the leptonic fraction x_{DU} , defined as [19, 60]:

$$x_{DU} = \frac{1}{1 + (1 + x_e^{1/3})^3}, \quad (19)$$

where $x_e = n_e/(n_e + n_\mu)$. For the models presented in this work, only pure nucleonic neutron stars enable DU process, and at very high density: 0.51 fm^{-3} , which imply a very massive star of $2.56 M_\odot$ as an inferior limit for the DU process.

We now display in Tab. III some macroscopic and microscopic properties of nucleonic and hyperonic neutron stars. As we have already pointed out, all star families have the same radius and tidal deformability for the canonical mass. Also, we need $\alpha < 0.75$ in order to reproduce a $2.50 M_\odot$ star. From the microscopic point of view, we can infer some features from the speed of the sound and the strangeness fraction. For instance, our study indicates that the central speed of the sound should be $v_s^2 > 0.62$ in order to produce at least a $2.50 M_\odot$. Such high value is almost twice the conformal limit imposed by pQCD [59]. In the same sense, we also need $f_s < 18\%$ at the core of the neutron star. When we look at the more well established $2.0 M_\odot$, we see that a strangeness fraction of only 3.6% is enough to prevent a formation of a $2.50 M_\odot$.

III. VECTOR MIT BAG MODEL

Let's now consider the possibility of the mass-gap object of the GW190814 being a stable quark star, sometimes called strange star. This idea is based on the so-

called Bodmer-Witten hypothesis [10, 11]. According to it, the matter composed of protons and neutrons may be only meta-stable. The true ground state of strongly interacting matter would therefore consist of strange matter (SM), which in turn is composed of deconfined up, down

Model	M_{max}/M_0	R (km)	n_c (fm $^{-3}$)	f_{sc}	v_{sc}^2	M_{DU}/M_\odot	$R_{1.4}$ (km)	$\Lambda_{1.4}$	$f_{s2.0}$
SU(6)	2.36	12.56	0.777	0.210	0.56	-	13.38	644	0.056
$\alpha = 0.75$	2.46	12.59	0.762	0.181	0.62	-	13.38	644	0.036
$\alpha = 0.50$	2.57	12.70	0.736	0.133	0.68	-	13.38	644	0.025
$\alpha = 0.25$	2.64	12.75	0.720	0.093	0.74	-	13.38	644	0.014
Nucl.	2.75	12.87	0.699	-	0.79	2.56	13.38	644	-
Constraints	> 2.50	-	-	-	< 1.0	> 1.50	12.2 – 13.7	458 – 889	-

TABLE III. Nucleonic and hyperonic neutron star properties for different values of α and some astrophysical constraints.

and strange quarks. For the SM hypothesis to be true, the energy per baryon of the deconfined phase (for $p = 0$ and $T = 0$) is lower than the nonstrange infinite baryonic matter. Or explicitly [10, 11, 61]:

$$E_{(uds)}/A < 930 \text{ MeV}, \quad (20)$$

at the same time, the nonstrange matter still need to have an energy per baryon higher than the one of nonstrange infinite baryonic matter, otherwise, protons and neutrons would decay into u and d quarks:

$$E_{(ud)}/A > 930 \text{ MeV}. \quad (21)$$

Therefore, both, eq. (20) and (21) must simultaneous be true.

One of the simplest model to study quark matter is to so called MIT bag model [62]. This model considers that each baryon is composed of three non-interacting quarks inside a bag. The bag, in turn, corresponds to an infinity potential that confines the quarks. In this simple model the quarks are free inside the bag and are forbidden to reach its exterior. All the information about the strong force relies on the bag pressure value, which mimics the vacuum pressure. However, the maximum mass of a stable quark star in the original MIT bag model is way below $2.50 M_\odot$. We can overcome this issue by using a modified MIT bag model which adds a massive repulsive vector field, analogous to the ω meson of the QHD. We follow this path here. The Lagrangian of the modified MIT bag model reads [61]:

$$\mathcal{L}_{vMIT} = \{\bar{\psi}_q[\gamma^\mu(i\partial_\mu - g_{qV}V_\mu) - m_q]\psi_q + \frac{1}{2}m_V^2 V_\mu V^\mu - B\}\Theta(\bar{\psi}_q\psi_q). \quad (22)$$

where m_q is the mass of the quark q of flavor u , d or s . Here, we follow ref. [61] and use ($m_u = m_d = 4 \text{ MeV}$, $m_s = 95 \text{ MeV}$); ψ_q is the Dirac quark field, B is the constant vacuum pressure, and $\Theta(\bar{\psi}_q\psi_q)$ is the Heaviside step function to assure that the quarks exist only confined to the bag. The quark interaction is mediated by the massive vector channel V_μ analogous to the ω meson in QHD [16]. Besides, leptons are added to account for β stable matter. Imposing MFA, and applying Euler-Lagrange to Eq. (22), we obtain the energy eigenvalue for the quark, as well as the expected value for the vector field.

$$E = \sqrt{m_q^2 + k^2} + g_{qV}V_0, \quad (23)$$

$$m_V^2 V_0 = \sum_q g_{qV} n_q,$$

where n_q is the number density of the quark q . Now, applying Fermi-Dirac statistics, the energy density is analogous to the QHD plus the bag term:

$$\epsilon = \sum_q \frac{N_c}{\pi^2} \int_0^{k_f} dk k^2 \sqrt{k^2 + m_q^2} + \frac{1}{2} m_V^2 V_0^2 + B + \sum_l \frac{1}{\pi^2} \int_0^{k_f} dk k^2 \sqrt{k^2 + m_l^2}, \quad (24)$$

where N_c is the number of colours and $p = \mu n - \epsilon$.

The interaction of the vector field with different quark flavors can follow two different prescriptions. In the first one we have an universal coupling, i.e. the strength of the interaction is the same for all three quarks. This is a more conventional approach, and was done, for instance, in ref. [63, 64]. In this case, $g_{uV} = g_{dV} = g_{sV}$. Another possibility explored in ref. [61] is that the vector field is not only analogous to the ω meson, but it is the ω meson itself. In this approach we can use symmetry group arguments and construct an invariant Lagrangian. In this approach we have: $g_{uV} = g_{dV}$ and $g_{sV} = 0.4g_{uV}$. We now follow ref. [61] and define two quantities:

$$G_V \equiv \left(\frac{g_{uV}}{m_V}\right)^2 \quad \text{and} \quad X_V \equiv \frac{g_{sV}}{g_{uV}}, \quad (25)$$

G_V is related to the absolute strength of the vector field itself; X_V is related to the relative strength of the vector field. If $X_V = 1.0$ we are dealing with an universal coupling, while $X_V = 0.4$ implies symmetry group arguments. We study how different values of G_V and X_V affect the macroscopic properties of strange stars.

Now, for a chosen value of G_V and X_V , the bag pressure B is not arbitrary. To predict the existence of strange stars, B must be chosen in order to satisfy both Eq. (20) and Eq. (21). The set of values that satisfies both equations simultaneous is used to construct the stability window [10, 11]. We display the stability window

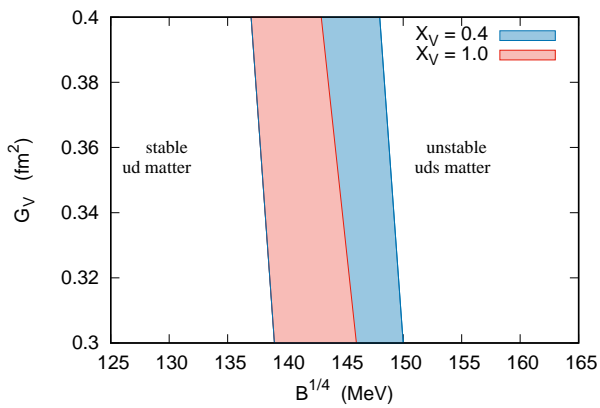


FIG. 6. (Color online) Stability window for $X_V = 1.0$ and $X_V = 0.4$

G_V (fm ²)	X_V	$B_{Min}^{1/4}$ (MeV)	$B_{Max}^{1/4}$ (MeV)
0.30	0.4	139	150
0.32	0.4	138	149
0.36	0.4	138	148
0.40	0.4	137	148
0.30	1.0	139	146
0.32	1.0	138	145
0.36	1.0	138	144
0.40	1.0	137	143

TABLE IV. Stability windows obtained with the vector MIT bag model.

for $0.30 \text{ fm}^2 < G_V < 0.40 \text{ fm}^2$ in Fig. 6 and the numerical results are shown in Tab. IV.

We can see that the lower limit of the stability window is independent of the value of X_V . This is expected, once it is related to the stability of the two flavored quark matter, expressed in eq. (21). On the other side, the stability of three flavored quark matter depends on the X_V . The stability window is always wider for $X_V = 0.4$, once the repulsion in the strange quark is lower, reducing the energy per baryon. We now show in Fig. 7 the EoS and the mass-radius relation for strange stars with $X_V = 1.0$ and $X_V = 0.4$. For $X_V = 1.0$, we plot the EoS and the TOV solution for both, minimum and maximum values of the bag as presented in Tab. IV. As can be seen, for a given bag value, the higher the value of G_V , the stiffer is the EoS and consequently, the higher is the maximum mass. For $X_V = 1.0$, a maximum mass above $2.50 M_\odot$ is reached for the minimum bag value for all three values of G_V presented in this work. In the case of the maximum bag value of Tab. IV, we see that only $G_V > 0.32$ can reach at least $2.50 M_\odot$. For $X_V = 0.4$, we plot the results only for the minimum bag value. We see that the EoS is softer when compared with $X_V = 1.0$, and

therefore produces lower values for the maximum mass, and only values $G_V > 0.32 \text{ fm}^2$ can reach at least $2.50 M_\odot$.

Another important constraint is the radius of the $1.4 M_\odot$ star. Considering only the results that reach at least $2.50 M_\odot$, the radii shown in Fig. 7 lie between 11.59 km and 12.58 km. We see that several radii agree with the NICER results [51, 52], Bayesian analysis [49, 50], as well as with ref. [8]. However, as we use here the results coming from ref. [1] as the main constraint, not all radius values are in the range between 12.2 km and 13.7 km. Indeed, neither stars produced with the maximum bag value nor stars with $G_V = 0.32 \text{ fm}^2$ have a radius above 12.2 km.

Now we check the values of the dimensionless tidal parameter Λ . As pointed in ref. [15, 58], the value of y_R in Eq. (14) must be corrected, since strange stars are self-bound and present a discontinuity at the surface. Therefore we must have:

$$y_R \rightarrow y_R - \frac{4\pi R^3 \Delta\epsilon_S}{M}, \quad (26)$$

where R and M are the star radius and mass respectively, and $\Delta\epsilon_S$ is the difference between the energy density at the surface ($p=0$) and the exterior of the star (which implies $\epsilon=0$). The results for $X_V=1.0$ and $X_V=0.4$ are plotted in Fig. 8:

As can be seen for $X_V=0.4$, only $G_V = 0.32 \text{ fm}^2$ fulfills the constraint for $\Lambda_{1.4}$ coming from ref. [1]. However, since its maximum mass is below $2.50 M_\odot$, we can rule out the possibility of the mass-gap object of the GW190814 event being a strange star with $X_V=0.4$. In the case of $X_V=1.0$, only the values of the maximum allowed bag fulfill the constraint. However, as pointed out earlier, these values present low radii, in disagreement with ref. [1]. We cannot completely rule out the possibility of the mass-gap object of the GW190814 being a strange star, since the radii values still fulfill NICER constraints. Nevertheless, in order to keep internal coherence, in the light of the constraints presented in ref. [1], we assert that the probability of the mass-gap object being a strange star is significantly lower than that of being a hadronic star.

In fig. 9, we display the speed of the sound. As can be seen, the causality $v_s^2 < 1$ is always satisfied. However, the conformal limit $v_s^2 < 1/3$ is violated, even at low densities. Nevertheless, we are far below the pQCD limit of $n > 40 n_0$. We finish this section displaying some macroscopic and microscopic properties of the strange stars in Tab. V. We only show results for $X_V=1.0$ as discussed in the text because for $X_V=0.4$ no parametrization is able to reach a $M > 2.50 M_\odot$ and $\Lambda_{1.4} < 889$ simultaneously.

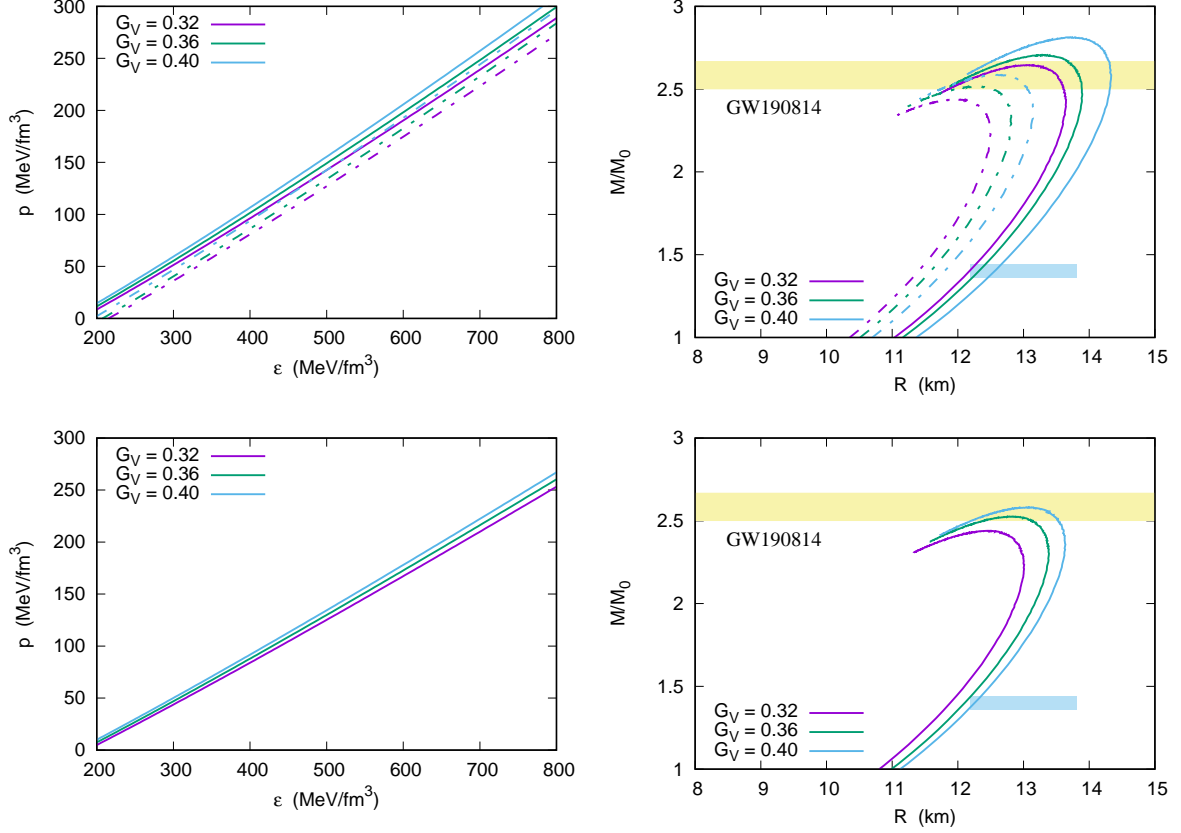


FIG. 7. (Color online) EoS (left) and TOV solution (right) for strange stars with $X_V = 1.0$ (top) and $X_V = 0.4$ (bottom). Solid lines indicate minimum bag value for the stability window and dotted lines indicate maximum bag value for the stability window.

G_V (fm ²)	$B^{1/4}$ (MeV)	M_{max}/M_0	R (km)	n_c (fm ⁻³)	$\Delta\epsilon_S$ (MeV/fm ³)	v_{sc}^2	$R_{1.4}$ (km)	$\Lambda_{1.4}$
0.32	138	2.64	13.14	0.699	180	0.50	12.17	983
0.36	138	2.70	13.30	0.671	174	0.51	12.31	1023
0.40	137	2.81	13.78	0.632	166	0.52	12.58	1072
0.32	145	2.44	11.96	0.794	216	0.51	11.40	634
0.36	144	2.51	12.26	0.759	208	0.52	11.59	729
0.40	143	2.58	12.57	0.725	198	0.53	11.80	817
Constraints	Stability window	> 2.50	-	-	-	< 1.0	12.2 – 13.7	458 – 889

TABLE V. Some strange star properties for $X_V = 1.0$ and some astrophysical constraints.

As can be seen, for the minimum bag value, the tidal parameter $\Lambda_{1.4}$ is close or even higher than 1000. We highlight here, that for $B^{1/4} = 144$ MeV and $G_V = 0.36$, we can produce a massive star with $M > 2.50 M_\odot$ with $\Lambda_{1.4} < 800$, agreeing with ref. [54], while the radius agrees with Bayesian analysis [49, 50] and the result presented in ref. [8]. Unlike the hadronic neutron star, we see that the central speed of the sound is only weakly linked to the stiffness of the EoS, being almost constant for all models.

IV. HYBRID STARS

We now investigate the possibility of the GW190814 event being a dynamically stable hybrid star. There are some questions we try to answer next: It is possible that the mass-gap object in the GW190814 event is a hybrid star? How do hyperons affect the presence of quarks in the neutron star core? What are the values of the chemical potential at the phase transition point? What are the maximum and minimum values of G_V that produce a dynamically stable hybrid star? What is the influence of the bag value? How does the factor X_V influence the

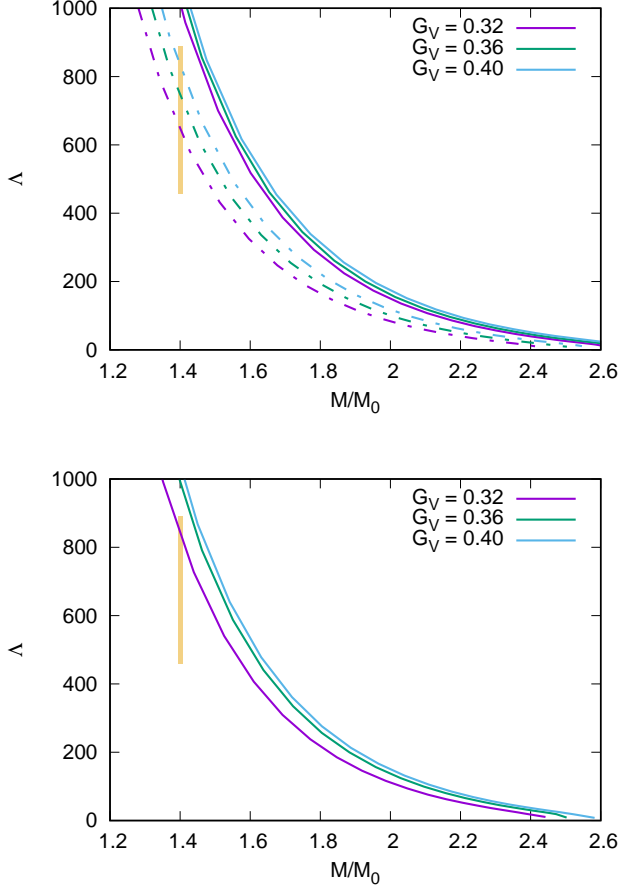


FIG. 8. (Color online) Dimensionless tidal parameter Λ for strange stars with $X_V = 1.0$ (top) and $X_V = 0.4$ (bottom). Solid lines indicate minimum bag value for the stability window and dotted lines indicate maximum bag value for the stability window.

macroscopic properties? What is the stellar minimum mass that presents a quark core? What are the size and the mass of the quark core in a stable hybrid star?

The possibility that the mass-gap object of the GW190814 event being a hybrid star has already been studied in ref. [6]. In that paper, the authors use the generic constant-sound-speed (CSS) parametrization, with no information about the quark interaction nor the chemical composition of the matter and the EoS reads [65]:

$$p(\epsilon) = a(\epsilon - \epsilon_0), \quad (27)$$

where a and ϵ_0 are constants related to the speed of the sound and the energy density at zero pressure, respectively. Here we use a more physical Lagrangian density based model described in Eq. (22).

Another difference between the present work and the study of ref [6] is the quark hadron phase transition criteria. In ref. [6] the transition pressure is treated as a

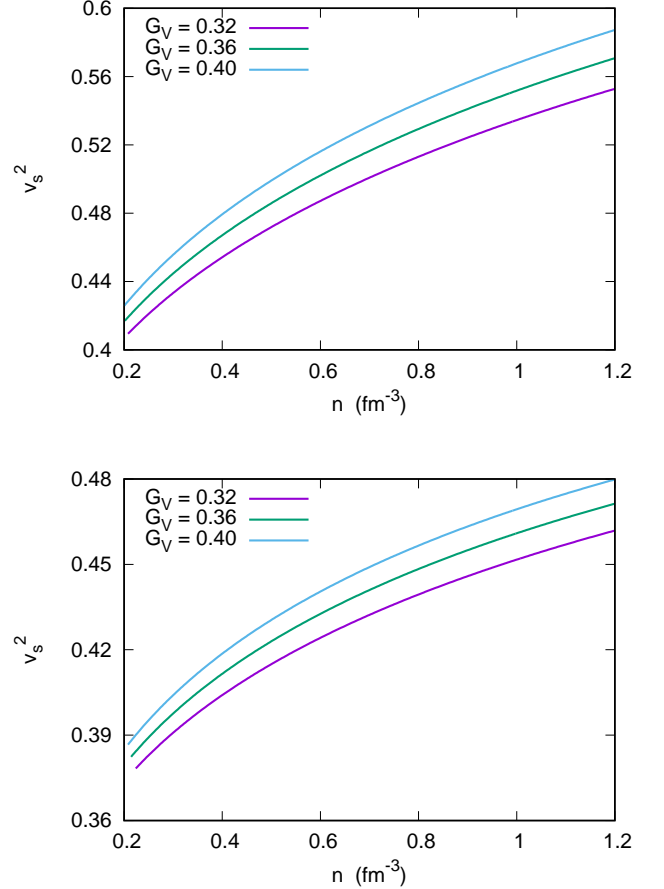


FIG. 9. (Color online) The square of the speed of sound with $X_V = 1.0$ (top) and $X_V = 0.4$ (bottom).

free parameter. We use the so called Maxwell construction, and the transition pressure is the one where the Gibbs free energy per baryon G/n_B of both phases intersect, being the energetically preferred phase the one with lower G/n_B [66]. The Gibbs free energy per baryon coincides with the baryon chemical potential, therefore we next call the intersection point as critical pressure and critical chemical potential. The Maxwell criteria read:

$$\mu_H = \mu_Q = \mu_C, \quad \text{at} \quad p_H = p_Q = p_C, \quad (28)$$

where the subscript H indicates a Hadronic phase, Q indicates quark phase and C indicates the critical values.

We begin by reanalysing the stability window of Fig. 6. To construct strange stars, we imposed that the energy per baryon of the deconfined phase was lower than the nonstrange infinite baryonic matter. But here we need the opposite. To produce a stable hybrid star, the strange matter must be unstable, otherwise, as soon as the core of the star converts into the quark phase, the entire star will convert into a quark star in a finite amount of time [67, 68]. Therefore we fix our bag values between $150 \text{ MeV} < B^{1/4} < 160 \text{ MeV}$ to ensure an unstable strange

matter. We study the possibility of a hybrid star with nucleons and quarks, and a hybrid star with nucleons, hyperons and quarks. To obtain very massive hybrid stars with nucleons and hyperons, we use next $\alpha = 0.25$. Now, for a chosen value of X_V , we solve the TOV equations for different values of G_V and of the bag. The values of G_V that produce a stable hybrid star with $M > 2.50 M_\odot$ form what we call the hybrid branch stability window.

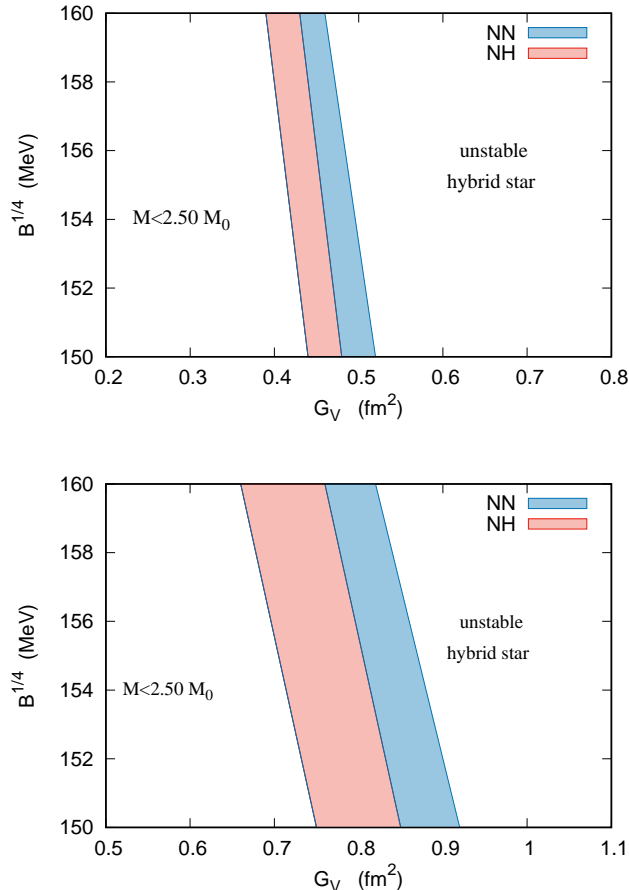


FIG. 10. (Color online) Hybrid branch stability window for $X_V = 1.0$ (top) and $X_V = 0.4$ (bottom) with a pure nucleonic EoS (NN) and an EoS with nucleons and hyperons (NH).)

We start by constructing the hybrid branch stability window for pure nucleonic (NN) and hyperonic (NH) EoS for the hadronic phase with $X_V = 1.0$ and $X_V = 0.4$. The results are presented in Fig. 10. We can see that for $X_V = 1.0$ and $150 \text{ MeV} < B^{1/4} < 160 \text{ MeV}$, the values of G_V that produce dynamical stable hybrid stars, with $M > 2.50 M_\odot$ lie between $0.39 \text{ fm}^2 < G_V < 0.48 \text{ fm}^2$ for a hybrid star with nucleons, hyperons and quarks, and $0.39 \text{ fm}^2 < G_V < 0.52 \text{ fm}^2$ for a hybrid star with only nucleons and quarks. With $X_V = 0.4$ the results are very different. The values of G_V now lie between $0.66 \text{ fm}^2 < G_V < 0.85 \text{ fm}^2$ for a hybrid star with nucleons, hyperons and quarks and $0.66 \text{ fm}^2 < G_V < 0.92 \text{ fm}^2$ for a hybrid star with only nucleons and quarks. We also

see that the hybrid branch stability window for $X_V = 0.4$ is significantly broader when compared with $X_V = 1.0$. The consequences of using a G_V below or above the values of the hybrid branch stability window are also different. If G_V is too low, stable hybrid stars still exist, however the maximum mass is lower than $2.50 M_\odot$. If G_V is too high, there is no dynamically stable hybrid star, yet the maximum mass is above $2.50 M_\odot$, but it is purely hadronic.

We also estimate the mass and size of the quark cores present in the most massive hybrid star of each model presented. To accomplish that, we follow ref. [42, 69] and solve the TOV equations [44] for the quark EoS from the density corresponding to the critical chemical potential up to the density at the maximum mass. The EoS and the TOV solution with $X_V = 1.0$ and $X_V = 0.4$ for the extreme values of G_V that satisfy the hybrid branch stability window are shown in Fig. 11, while the macroscopic and microscopic properties are displayed in Tab. VI.

Several different comparisons can be done from the results presented in Tab. VI. For instance, for a fixed value of B , X_V , and G_V we can see the influence of hyperons in hybrid stars. In this case, the presence of hyperons does not affect the maximum mass of a hybrid star. Indeed, hyperons soften the EoS and make the hadron-quark phase transition more difficult. A hybrid star family with only nucleons present a lower critical chemical potential, therefore a lower M_{min} , which is the minimum star that presents a quark core, and at the same time present a larger quark core when compared with the case with hyperons.

By increasing G_V we see that an increase of the maximum mass. However, as it also increases the critical chemical potential, the M_{min} becomes very close to the maximum mass. For the maximum allowed value of G_V , the mass and radius of the quark core are very small. Moreover, we see that nucleonic hybrid stars allow a higher value of G_V , and therefore produce a higher maximum mass.

For a correct choice of G_V , the maximum mass does not depend on the bag value. However, the mass and radius of the quark core do. Higher values of the bag produce lower sizes of the quark core, even for the lower value of G_V in the hybrid branch stability window.

The mass and size of the quark core strongly depend on the value of the critical chemical potential. Higher values of μ_C produce low values of the quark core. Massive quark cores can be obtained with low values of the bag and low values of G_V . We can also see that the critical chemical potential can be as high as 1700 MeV. This value is significantly higher than those around 1200 MeV presented in other studies about hybrid stars [69–71].

For a correct choice of G_V , the hybrid star maximum mass is independent of X_V . However $X_V = 0.4$ seems to produce a slightly lower value of the mass and radius of the quark core when compared with the ones obtained with $X_V = 1.0$.

The mass and radius of the quark core are strongly

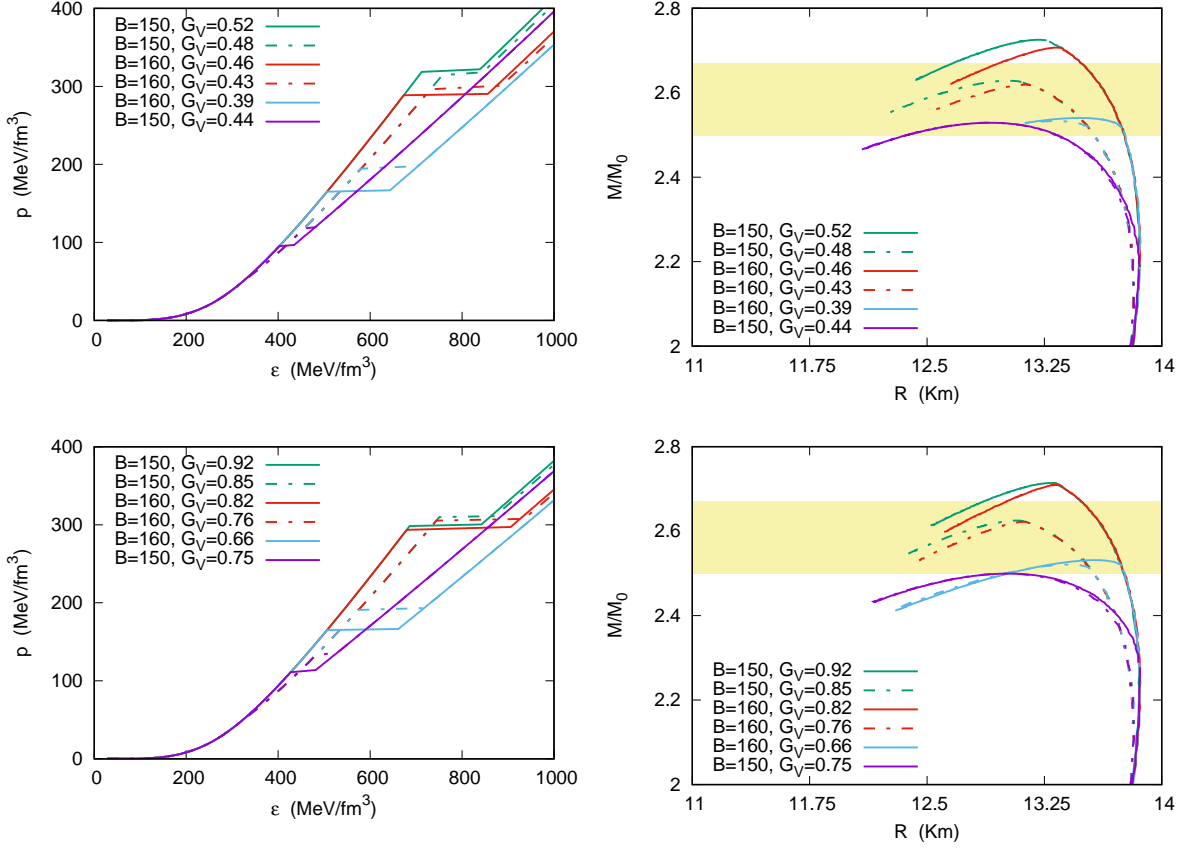


FIG. 11. (Color online) EoS (left) and TOV solution (right) hybrid stars with $X_V = 1.0$ (top) and $X_V = 0.4$ (bottom) at the extreme values of G_V . Solid lines indicate a hadronic phase with only nucleons (NN) and dotted lines indicate a hadronic phase with nucleons and hyperons (NH)

model dependent. The mass can vary from only $0.002 M_\odot$ to values larger than 1 solar masses. The quark core can vary from less than 1 km to almost 8 km. Also, we do not discuss the tidal deformability or the radius of the canonical mass, once in our model all hybrid stars have a mass of at least $2.18 M_\odot$.

We finish our analysis discussing the speed of the sound at the critical chemical potential in the light of the results presented in ref. [8]. The authors claim that the speed of the sound of the quark matter is closely related to

the mass and radius of the quark core in hybrid stars. Moreover, they assert that if the conformal bound ($v_s^2 < 1/3$) is not strongly violated, massive neutron stars are predicted to have sizable quark-matter cores. As can be seen, we do not find such correlation between the size of the quark core and the speed of sound. We are even able to produce a quark core with mass above 1 solar masses, with $v_s^2 = 0.50$, far above the conformal limit. Also, the most massive quark core is not those with the lower speed of the sound.

V. CONCLUSION

In this work we discuss the possibility of the mass-gap object in the GW190814 event being a degenerate object instead of a black hole. The main remarks are resumed as follows:

- We start by looking if there is a parametrization of the QHD that fulfills all symmetric nuclear mat-

ter constraints, as discussed in two review works (ref. [29, 30]) and, at the same time, produce stars that can reach at least $2.50 M_\odot$. We choose a modified version of the NL3* to accomplish this task.

- We then study in what conditions hyperons can be present in such massive neutron stars. We show that a hyperonic neutron star with mass above $2.50 M_\odot$ is possible if we use symmetry group arguments to fix the hyperon-meson coupling constant and use

X_V	$B^{1/4}$ (MeV)	Type	G_V (fm ²)	M_{max}/M_\odot	R (km)	n_c (fm ⁻³)	μ_C (MeV)	M_{min}/M_\odot	M_Q (M_\odot)	R_Q (km)	v_{SC}^2
1.0	150	NH	0.44	2.53	12.90	0.719	1336	2.28	0.874	7.23	0.50
1.0	150	NN	0.44	2.53	12.90	0.720	1280	2.18	1.064	7.89	0.49
1.0	150	NH	0.48	2.63	13.02	0.710	1707	2.62	0.029	2.08	0.55
1.0	150	NN	0.52	2.73	13.21	0.689	1736	2.72	0.019	1.82	0.57
1.0	160	NH	0.39	2.53	13.31	0.665	1499	2.51	0.125	3.55	0.51
1.0	160	NN	0.39	2.54	13.47	0.624	1445	2.50	0.148	3.87	0.51
1.0	160	NH	0.43	2.62	13.13	0.718	1680	2.62	0.009	1.35	0.54
1.0	160	NN	0.46	2.71	13.32	0.718	1683	2.70	0.043	2.36	0.55
0.40	150	NH	0.75	2.50	13.00	0.712	1373	2.35	0.650	6.44	0.48
0.40	150	NN	0.75	2.50	13.01	0.713	1321	2.27	0.817	7.08	0.47
0.40	150	NH	0.85	2.63	13.08	0.715	1695	2.62	0.015	1.66	0.51
0.40	150	NN	0.92	2.71	13.29	0.689	1703	2.71	0.011	1.50	0.51
0.40	160	NH	0.66	2.52	13.40	0.661	1490	2.51	0.087	3.14	0.48
0.40	160	NN	0.66	2.53	13.57	0.632	1444	2.51	0.115	3.53	0.48
0.40	160	NH	0.76	2.62	13.11	0.740	1689	2.62	0.002	0.85	0.50
0.40	160	NN	0.82	2.71	13.33	0.715	1695	2.71	0.004	1.11	0.51

TABLE VI. Maximum mass, radius, central density, critical chemical potential, M_{min} , mass and radius of the quark core and the speed of sound at the critical chemical potential for the extreme values of G_V that allows dynamical stable hybrid stars.

$\alpha < 0.75$.

- We show that the maximum mass, as well as the strangeness fraction are strongly linked to the choice of α . The lower the value of α , the lower the strangeness fraction, and the higher the maximum mass.
- The maximum mass is also linked with the speed of the sound at the core of the neutron star. The lower the α , the higher the speed of sound and, consequently the higher the maximum mass. The conformal limit ($v_s^2 < 1/3$) [59], is always violated.
- We discuss the minimum mass that enables DU process, in the light of the constraint $M_{DU} > 1.50M_\odot$ [60]. We see that only pure nucleonic neutron stars are able to undergo a DU process and only for stars with $M > 2.56M_\odot$.
- We also analyse the constraints related to the canonical $M = 1.40 M_\odot$ star. As hyperons are only present in stars with $M > 1.66 M_\odot$, all hadronic models present the same $R_{1.4} = 13.38$ km and $\Lambda_{1.4} = 644$. These values agree with the main constraint from ref. [1], i.e., $12.2 \text{ km} < R_{1.4} < 13.7$ and $458 < \Lambda_{1.4} < 889$.
- We then study the possibility of the mass-gap object being a self-bound quark star, satisfying the Bodmer-Witten conjecture [10, 11]. We construct the stability window for two values of X_V and show that for $X_V = 0.4$, no strange star is able to simultaneously fulfill $M > 2.50 M_\odot$ and $\Lambda_{1.4} < 889$.
- For $X_V = 1.0$ we are able to simultaneously fulfill $M > 2.50 M_\odot$ and $\Lambda_{1.4} < 889$, but with $R_{1.4} < 12.2$ km. This is in disagreement with the main constraint, but still in agreement with others results found in the literature [49–51].
- We finally analyse the possibility that the mass-gap object is a hybrid star. We discuss if such hybrid star can be composed by nucleons, hyperons and quarks, or by nucleons only and quarks. We show that for a correct choice of G_V , both possibilities can be satisfied. Also, we are able to produce hybrid stars for all values of the bag lying between 150 MeV and 160 MeV, for both $X_V = 1.0$ and $X_V = 0.4$
- For a fixed G_V , the presence of hyperons reduces the mass and radius of the quark core, but has little effect on the maximum mass of the hybrid star.
- The size and the mass of the quark core is strongly model depend, its mass vary from values lower than $0.01 M_\odot$ to values larger than $1.0 M_\odot$.
- We did not find a correlation between the speed of the sound of the quark matter and the size of the quark core, as suggested in ref. [8]. Nevertheless, we are able to produce a very massive quark core $M > 1 M_\odot$, even though the conformal limit is violated.

Acknowledgments: This work is a part of the project INCT-FNA Proc. No. 464898/2014-5. D.P.M. is partially supported by Conselho Nacional de Desenvolvimento Científico e Tecnológico (CNPq/Brazil) under grant 301155.2017-8.

- [3] H. Das, A. Kumar, S. Patra, Phys. Rev D **104**, 063028 (2021)
- [4] V. Dexheimer et al., Phys. Rev C **103**, 025808 (2021)
- [5] A. Sedrakian, F. Weber, J. Li, Phys. Rev D **102**, 041301(R) (2020)
- [6] S. Han, A. Steiner Phys. Rev D **99**, 083014 (2019)
- [7] I. Rather , A. Usmani, S. Patra, J. Phys G **48**, 085201 (2021)
- [8] E. Annala et al, Nat. Phys. **16**, 907 (2020)
- [9] J. Li, A. Sedrakian, F. Weber, Phys Lett. B **810**, 135812 (2020)
- [10] A. Bodmer, Phys. Rev. D **4**, 1601 (1971).
- [11] E. Witten, Phys. Rev. D **30**, 272 (1984).
- [12] I. Bombaci et al., Phys. Rev. Lett. **126**, 162702 (2021)
- [13] C. Zhang and R. B. Mann, Phys. Rev. D **103**, 063018 (2021).
- [14] M. Albino, R. Fariello, F. Navarra, Phys. Rev. D **104**, 083011 (2021)
- [15] O. Lourenço, et al., Phys. Rev. D **103**, 103010 (2021)
- [16] B. D. Serot, Rep. Prog. Phys. **55**, 1855 (1992)
- [17] F. Fattoyev et al., Phys. Rev. C **82**, 055803 (2010)
- [18] J. Boguta, A. Bodmer, Nucl. Phys. A **292**, 413 (1977)
- [19] R. Cavagnoli, D. P. Menezes, C. Providencia, Phys. Rev. C **84**, 065810 (2011)
- [20] V. Dexheimer et. al, J. Phys. G **46**, 034002 (2019)
- [21] L. Lopes, D. Menezes, Eur. Phys. J. A **56**, 122 (2020)
- [22] S. Weissenborn, D. Chatterjee, J. Schaffner-Bielich, Nucl. Phys. A **881**, 62 (2012)
- [23] T. Miyatsu and M. Cheoun, Phys. Rev. C **88**, 015802 (2013).
- [24] M. Wang, et al., Chin. Phys. C **36**, 1603 (2012)
- [25] S. Shlomo, V. Kolomietz, G. Colo, Eur. Phys. J. A **30**, 23 (2006)
- [26] P. Reinhard and W. Nazarewicz, Phys. Rev. C **87**, 014324 (2013)
- [27] E. De Filippo and A. Pagano, Eur. Phys. J. A **50**, 32 (2014)
- [28] N. K. Glendenning, *Compact Stars*, Springer, New York - Second Edition (2000)
- [29] M. Dutra et al., Phys. Rev. C **90**, 055203 (2014)
- [30] M. Oertel et al., Rev. Mod. Phys. **89**, 015007 (2017)
- [31] N. Paar et al., Phys. Rev. C **90**, 011304 (2014)
- [32] J. Lattimer, Y. Lim, Astrophys. J. **771**, 51 (2013)
- [33] J. Lattimer, A. Steiner, Eur. Phys. J. A **50**, 40 (2014)
- [34] J. Estee, et al., Phys. Rev. Lett. **126**, 162701 (2021)
- [35] B. Reed, et al., Phys. Rev. Lett. **126**, 172503 (2021)
- [36]] G. Lalazissis, J. König, P. Ring, Phys. Rev. C **55**, 540 (1997).
- [37] Bo-Lin Li et. al, J. Phys. G **49**, 045201 (2022)
- [38]] G. Lalazissis et al., Phys. Lett. B **36**, 671 (2009).
- [39]] M. Rashdan, Phys. Rev. C **63**, 044303 (2001).
- [40] H. C. Das et al., Int. J. Mod. Phys. E **30**, 2150088 (2021)
- [41] T. Inoue, JPS Conf. Proc. **26**, 023018 (2019)
- [42] L. Lopes, D. Menezes, Nucl. Phys. A **1009**, 122171 (2021)
- [43] L. Lopes, D. Menezes, Phys. Rev C **89**, 025805 (2014)
- [44] J. R. Oppenheimer, G. M. Volkoff, Phys. Rev. **55**, 374 (1939)
- [45] G. Baym, C. Pethick, P. Sutherland, Astrophys. J. **170**, 299 (1971)
- [46] F. Ozel, et al., Astrophys. J. **820**, 28 (2016)
- [47] C. Capano, et al., Nat. Astron. **4**, 625 (2020)
- [48] J. Lattimer, A. Steiner, Astrophys. J. **784**, 123 (2014)
- [49] Y. Li et al., Eur. Phys. J. A **57**, 31 (2021)
- [50] M. Coughlin et al., Mon. Not. Roy. Astr. Soc. Lett. **489**, L91 (2019)
- [51] T. Riley, et al., Astrophys. J. Lett. **887**, L21 (2019)
- [52] M.C. Miller, et al., Astrophys. J. Lett. **887**, L24 (2019)
- [53] E. Annala et al., Phys. Rev. Lett. **120**, 172703 (2018)
- [54] B. Abbott et al., Phys. Rev. Lett. **121**, 161101 (2018)
- [55] C. Flores et al., Eur. Phys. J. C **80**, 1142 (2020)
- [56] K. Chatziioannou, Gen. Rel. Grav. **52**, 109 (2020)
- [57] B. Abbott et al., Phys. Rev. Lett. **119**, 161101 (2017)
- [58] S. Postnikov, M. Prakash, J. Lattimer, Phys. Rev. D. **82**, 024016 (2010)
- [59] P. Bedaque and A. Steiner Phys. Rev. Lett. **114**, 031103 (2015)
- [60] T. Klahn et al., Phys. Rev. C **74**, 035802 (2006)
- [61] L. Lopes, C. Biesdorf, D. Menezes, Phys. Script. **96**, 065303 (2021)
- [62] A. Chodos et al., Phys. Rev. D **9**, 3471 (1974)
- [63] R. Gomes et al., Mon. Not. Roy. Astron. Soc. **485**, 4873 (2019)
- [64] R. Gomes, P. Char, and S. Schramm, Astrophys. J. **877**, 19 (2019)
- [65] J. Zdunik, P. Haensel, Astron. & Astrophys. **551**, A61 (2013)
- [66] N. Chamel et al., Astron. & Astrophys. **553**, A22 (2013)
- [67] A. Olinto, Phys. Lett. B **192**, 71 (1987)
- [68] K. Marquez, D. Menezes JCAP **12**, 028 (2017)
- [69] L. Lopes, C. Biersdorf, D. Menezes, Mon. Not. Roy. Astr. Soc. **512**, 5110 (2021)
- [70] T. Klahn, T. Fischer, M. Hempel, Astrophys. J. **836**, 89 (2017)
- [71] A. Ayriyan al., Phys. Rev. C **97**, 045802 (2018)